



Micromechanical damage behavior of fiber-reinforced composites under transverse loading including fiber-matrix debonding and matrix cracks

Mohammad Palizvan · Mohammad Tahaye Abadi · Mohammad Homayoune Sadr 

Received: 23 July 2019 / Accepted: 18 September 2020 / Published online: 31 October 2020
© Springer Nature B.V. 2020

Abstract This paper examines the micromechanical damage behavior of carbon-epoxy composite using representative volume elements (RVEs). An algorithm is developed to generate random distributions of fibers in the RVE, and it is possible to create a fiber distribution with high fiber volume fractions. Fiber-matrix debonding and matrix crack are considered as the dominant damage modes. The fiber material is considered linear elastic and Drucker–Prager’s plastic criterion coupled with progressive damage behavior is assumed for matrix material. Moreover, cohesive elements are considered to model fiber-matrix debonding. The effects of different parameters such as fiber volume fraction, random fiber distribution, normal radii distribution, various cohesive parameters, and minimum fiber neighboring spacing on the overall damage behavior of the RVE, mostly the regime beyond the peak stress, are described in detail. It is concluded that due to the high-stress concentration regions, smaller elements are needed to analyze the high fiber volume fractions RVEs accurately. The peak stress and the corresponding strain are insensitive to microstructural randomness. Furthermore, the RVEs’ final failure strain is highly dependent on different fiber arrange-

ments layouts. Since the RVEs are under transverse strain, normal cohesive strength is the dominant cohesive zone parameter that has a significant role in the damage behavior of RVEs. It is shown that minimum fiber neighboring spacing affects the strain in which matrix crack initiates.

Keywords RVE · Fiber-matrix debonding · Matrix crack · Damage mechanics · Composite material

1 Introduction

Fiber reinforced composite materials have been applied in a wide range of structural applications (Hollaway 2010), especially in the aerospace industry (Soutis 2005), as they have strong mechanical performance. The mechanical response of composite materials may be affected by several damage mechanisms in which the fiber-matrix debonding and matrix cracks are of primary damage modes. Although the initiation and propagation of these damage modes will not directly cause the collapse of the structure, they will instantly decrease the strength of the damaged layer to a specific limit. Experimental researches have confirmed that the primary damage mechanism associated with transverse fiber direction is debonding occurring at the fiber-matrix interface (Gamstedt and Sjögren 1999; Thomas 2006).

Due to the damage behavior complexity, many micromechanical investigations have concentrated on transverse fracture behavior from the standpoint of

M. Palizvan · M. H. Sadr (✉)
Aerospace Engineering Department, Amirkabir University
of Technology, Tehran, Iran
e-mail: sadr@aut.ac.ir

M. Tahaye Abadi
Aerospace Research Institute, Ministry of Science, Research and
Technology, Tehran, Iran

damage initiation (Masaki 2009; Asp et al. 1996). Several earlier studies have made the hypothesis of a periodic fiber arrangement in the microstructure (Thomas 2006; Maligno 2008), which following various studies, may not be representative of actual material behavior (Masaki 2009; Trias 2006). However, numerous advanced micromechanics damage models have been developed, such as those by González and LLorca (2007), Totry et al. (2008), which enable the prediction of microscopic damage progression and the final failure of carbon fiber epoxy composites. These have been accomplished through the use of cohesive zone models at the fiber-matrix interfaces coupled with non-linear constitutive material models to represent the behavior of the constituent materials.

The fiber radius is considered as a significant parameter affecting the behavior of the RVE. Although many previous investigations are based on the hypothesis of the identical fiber radii (Asp et al. 1996; Maligno 2008; Trias 2006; González and LLorca 2007; Totry et al. 2008), Vaughan and McCarthy (Vaughan and McCarthy 2010) accentuated that the fibers radii are not identical and have a normal distribution by experimental imaging as shown in Fig. 1. Thus, the normal distribution of radii should be taken into account in the micromechanical analyses to obtain a more accurate conclusion. In the following, Ismail et al. (2016) examined the elastic behavior of composites with the assumption of a normal distribution for the fiber radius and studied the effective elastic properties and the range of changes using RVEs with random fiber distributions.

Although various types of research (Zhang et al. 2019; Baby 2015; Soni 2014) have been implemented, the damage initiation and propagation mechanisms in microscale are still not well understood. Although the ultimate goal of the project is to derive a flow rule for damage behavior of composite material for macro-scale models, as Zhang et al. (2019), Baby (2015), which helps us to calculate the damage parameters without analyzing any micro-scale, in this paper, the focus is only on the micromechanical damage behavior of composite RVEs. Zhang et al. (2019), Baby (2015) shown that it is essential to know when the damage parameters begin to increase from zero (the climax of the micro-scale response) and how they reach to one during the loadings (the portion after the peak) to identify damage flow rule constants. This proportion (in which damage parameter shift from 0 to 1) is the equivalent part of diagrams in which the matrix cracks

and fiber-matrix debonding has been created and propagated. It is noteworthy that the micro-scale models represent integration points in the macro-scale analysis. So, the complete loss of strength in the micro-scale brings about a local failure in the macro scale, not the ultimate failure. For instance, it may represent a crack initiation in that integration point.

The current work is an extension of the investigation by Ismail et al. (2016) on the mechanical behavior of composite RVE subjected to transverse tension. The representative volume element consisting of fiber, matrix, and the interface was established for the simulation, considering random fiber distribution. The two dominant damage mechanisms of fiberreinforced composites, including both fiber-matrix debonding and matrix cracking, were taken into account with the normal radii distribution hypothesis for fibers. Moreover, periodic boundary conditions were applied to the RVEs. The paper is organized into six sections. The second section provides details on the generation of random RVEs. The Finite element analysis features are detailed in the third section. The material properties are presented in the fourth section. The discussion of results and conclusions are presented in the fifth and sixth sections, respectively.

2 Generation of random RVEs

RVE with random fiber distribution can represent a more realistic microstructure of fiber-reinforced composites. Randomness can cause stress concentration where the fibers are near each other and will radically affect the plastic and damage behavior of the RVE. The program code is developed in MATLAB software, and then the files are used to generate RVE with random fiber distribution in Abaqus.

Most of the time a square or rectangular RVE has been used for investigating the micromechanical behavior of composite materials.

Several researchers developed algorithms to generate RVEs with high fiber volume fractions (Melro 2011; Romanov et al. 2013). Melro (2011) move the existing fibers to the center of the RVE incrementally to provide free space for subsequent fibers. Moreover, they investigated several geometrical statistical characterizations such as Nearest neighbour distance, Nearest neighbour orientation, Ripley's K function, and Pair distribution function (Melro 2011; Romanov et al. 2013). More-

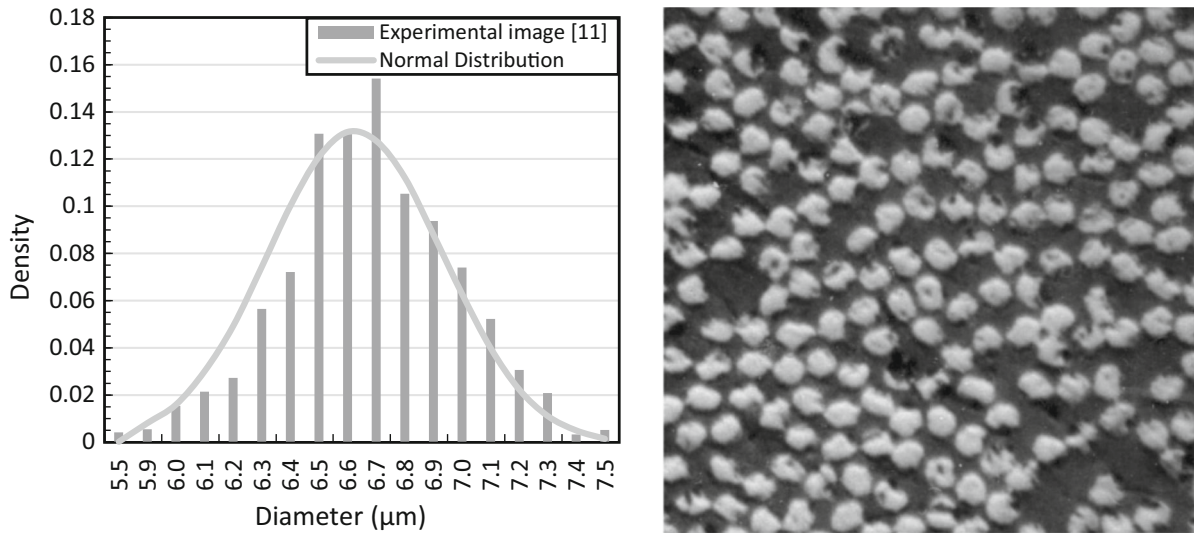


Fig. 1 Normal distribution of fiber radii introduced by [Vaughan and McCarthy \(2010\)](#)

over, it was concluded that in RVEs with random fiber distribution, the maximum strength is higher than RVEs with hexagonal and rectangular fiber arrangements, and also, the damage initiation and final failure occur in elder strains. So, the fracture energy of the RVE, which can be derived from the area below the stress-strain curve, increases.

Other researchers like [Mishnaevsky and Gaoming \(2014\)](#) investigated the effect of microstructure of hybrid carbon/glass fiber composites on their strength. They also consider the effect of fiber clustering in the damage behavior of the RVE. Like [Romanov et al. \(2013\)](#), they consider Ripley's K function, and Pair distribution function to testify the randomness of the fiber distribution in the RVE. They conclude that the strain of the RVE when it diminishes 50% of its strength is decreased by increasing fiber volume fraction. As the maximum stress level of the RVE is remain mostly constant, so by increasing the fiber volume fraction, the fracture energy of the RVE is reduced.

In the present work, for generating RVE with high fiber volume fractions, the fibers are posed besides each other with the minimum fiber neighboring distance to produce the desire fiber volume fraction, then fibers randomly move incrementally in arbitrary directions in the RVE to obtain random distributions.

3 Finite element analysis

Finite element (FE) analysis was implemented using ABAQUS ([Abaqus 2003](#)). The two-dimensional 3-node and 4-node bilinear plane strain elements (CPE3, CPE4) were opted to mesh the fibers and the matrix. Also, Python scripts have been written to generate and scatter fibers in the FE models of the RVEs. Abaqus implicit has been employed for the analyses and in some cases viscosity parameter and the line search algorithm has been enabled.

According to the investigations carried out by [Vaughan and McCarthy \(2010\)](#), the fiber radius was considered as a normal distribution with a mean value of 6.6 μm and a standard deviation of 0.3106. A new algorithm is taking into account the random fiber distributions. Moreover, the minimum neighboring distance 0.8 μm is considered to generate random fiber distributions.

The significance of periodic boundary conditions in the micromechanical analysis has been illustrated by several authors ([Xia et al. 2003](#); [Nguyen 2012](#); [Barbero 2013](#)). The boundary conditions and the fiber distributions are both considered periodic in this research. In other words, the layouts of the fibers are in a way that the fibers on the opposite sides complement each other. This is a prerequisite for performing periodic boundary conditions. To this end, the displacement of the nodes

in one edge is related to the displacement of the corresponding nodes on the opposite edge.

Another significant parameter is the dimension of the RVE. Daniel (2006) pointed out that the minimum size of an RVE, which can represent the behavior of the composite material with reasonable accuracy, is fifty times more than fiber radii in RVE with 50% fiber volume fraction. The dimensions of the RVEs in this study are modeled in the same way as the research (Yang 2013; Melro et al. 2008), which is fifty times the radius of the fiber, a $165 \times 165 \mu\text{m}$ square.

There are several theories presented to calculate the efficacious material properties, such as Mean-field approaches and numerical homogenization. Mean-Field Approaches and similar techniques (Clyne and Hull 2019; Böhm 2020) Profoundly idealized micro-scale models are used (like considering a unit cell with fiber in the center), and the microscale models within each constituent are approximated by their phase means $\langle \varepsilon \rangle^{(p)}$ and $\langle \sigma \rangle^{(p)}$, i.e., an identical stress and strain distributions are applied. The phase characteristics employ these models via statistical descriptors, such as fiber volume fractions, microscale symmetry models, fiber aspect ratios, etc. In Mean-Field Approaches the localization relationships practice the form

$$\begin{aligned} \langle \varepsilon \rangle^{(p)} &= \bar{A}^{(p)} \langle \varepsilon \rangle \\ \langle \sigma \rangle^{(p)} &= \bar{B}^{(p)} \langle \sigma \rangle \end{aligned} \quad (1)$$

where (p) stands for the matrix or inclusion phase of the material. It is noteworthy that the phase concentration tensors \bar{A} and \bar{B} used in Mean-Field Approaches are not functions of the spatial coordinates. Mean-field approaches attempt to be expressed (and implement approximations for efficacious material properties) in terms of the phase concentration tensors, and they have been profoundly robust in explaining the thermoelastic response of inhomogeneous materials with low computational costs. Their most significant aspects are efficacious field and medium estimates. It is a remarkable note that the analytical equations never can consider all micromechanical characteristics like fiber arrangements, fiber shapes, minimum fiber neighbouring distance or fiber radii etc. so definitely micromechanical analyses are needed to achieve a reliable characteristic for composite materials.

However, in this study, the numerical homogenization relationships for the stress and strain tensors are derived by Eq. 2, known as the average strain and aver-

age stress formulas

$$\begin{aligned} \langle \varepsilon \rangle &= \frac{1}{A_s} \int_{V_s} \varepsilon(x) dA \\ \langle \sigma \rangle &= \frac{1}{A_s} \int_{V_s} \sigma(x) dA \end{aligned} \quad (2)$$

where the A_s is the surface of the domain “s”.

For results validation, the readers are referred to our previous study (Palizvan et al. 2020) where the modeling technique and the analyses performed by the authors have been validated by presented results of Yang (2012) about fiber-matrix interface debonding and matrix cracking in an RVE.

4 Material behavior

As fiber fracture is unlikely to occur under transverse loadings (Yang 2012), the carbon fibers are assumed to be linear elastic and no damage model has been implemented for the fibers. The mechanical properties used in the analysis for AS4 carbon fiber with 3501-6 epoxy matrix were taken from Melro (2011) and are given in Table 1.

Several experimental studies have confirmed that fiber-matrix debonding and matrix cracks are the two dominant damage modes in micromechanical RVEs in composite materials under transverse loadings (Soden et al. 1998; Vaughan and McCarthy 2011). Consequently, the damage behavior of the epoxy and the interface are considered, which is illustrated in detail in the following. As epoxy is sensitive to the hydrostatic stress (Asp et al. 1996, 1995), the matrix is assumed to behave as an isotropic, elastic–plastic solid with the Drucker-Prager yield criterion. It is observed that the behavior of epoxy is sensitive to the hydrostatic stress which implies that materials become stronger with increasing pressure; their compressive yield stresses are higher than tensile yield stresses (Guild 2004).

Table 1 Transverse mechanical properties of the carbon and epoxy resin (Melro 2011)

	Carbon fiber	Epoxy resin
Young’s modulus (GPa)	13	3.35
Poisson ratio	0.2	.35
Tensile strength (MPa)	–	80
Compressive strength (MPa)	–	12

Drucker–Prager model allows epoxy to harden isotropically and is able to simulate inelastic dilation and volume change with inelastic behaviour and flow rule. Several authors used Drucker–Prager or Mohr–Coulomb criteria to capture this phenomenon (Yang 2015, 2016; Han 2015). Therefore, without considering these criteria, the RVEs’ responses would lead to unreliable results especially in RVEs under component loadings. Moreover, using the elastic-perfectly plastic model results that nonlinear behavior occurs at a higher strain and will predict a lower overall strength for the RVE.

The Drucker–Prager yield criterion is expressed by the following equation

$$F = t - p \tan \beta - d = 0,$$

$$t = \frac{1}{2}q \left[1 + \frac{1}{k} - \left(1 - \frac{1}{k} \right) \left(\frac{r}{q} \right)^3 \right] \quad (3)$$

where p , q , r , β , d , and k are the equivalent pressure stress, the Mises equivalent stress, the third invariant of deviatoric stress, the slope of the linear yield surface in the p – t stress plane (the friction angle of the material), and the cohesion of the material, and the ratio of the yield stress in triaxial tension to the yield stress in triaxial compression, respectively.

The parameters required for the Abaqus modeling, β and k can be defined by the ensuing equations

$$\tan \beta = \frac{6 \sin \varphi}{3 - \sin \varphi} \quad (4)$$

$$k = \frac{3 - \sin \varphi}{3 + \sin \varphi} \quad (5)$$

where φ can be obtained as

$$\sin \varphi = \frac{\sigma_{mc} - \sigma_{mt}}{\sigma_{mc} + \sigma_{mt}} \quad (6)$$

The matrix elastic constants are listed in Table 1 and the parameters of Drucker–Prager yield criterion are $\varphi = 11.5^\circ$, $\beta = 23.2^\circ$ and $k = 0.875$ (Yang 2015), which makes the maximum tensile and compression strength have the values of $\sigma_{mt} = 80$ and $\sigma_{mc} = 120$ MPa, respectively.

Apart from the plastic criterion for the matrix, a criterion to predict the initiation and propagation of damage is also required. In this study, due to the investigation by Yang (2016), the equivalent plastic strains at damage initiation for uniaxial tension and compression are assumed as 0.025 and 0.25, respectively. After the initiation of matrix failure, the damage growth is introduced by a progressive failure procedure, based on

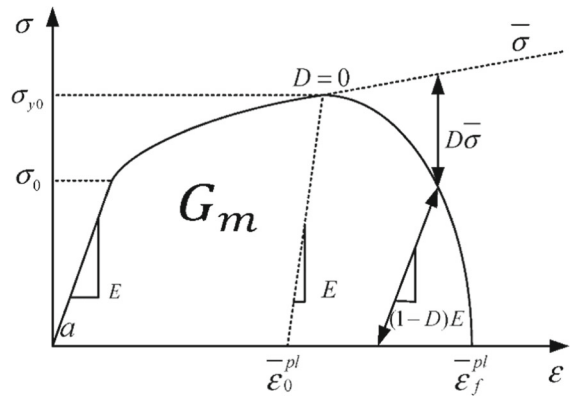


Fig. 2 The damage behavior of Epoxy

energy criterion, with the fracture energy of the matrix defined as $G_m = 0.005$ N/mm (Yang 2016), as shown in Fig. 2.

The dashed curve in Fig. 2 is the stress-strain response in the absence of damage, while the solid curve expresses the damaged response. The damage exhibits itself in both softening of the yield stress and degradation of the elasticity, which are related to the damage variable D , which increases with an increase in loading.

The cohesive zone modeling (CZM) is the most common approach for fiber-matrix damage problems. Generally, crack or damage initiates when the displacement or force reaches interfacial strength. Then the critical fracture energy controls the displacement for forming the complete crack.

Unlike the cohesive strength and fracture energy, the specific shape chosen for the cohesive model does not have much effect on the results. Most damage models, such as Camanho et al. (2003), Turon (2006), and Dávila et al. (2009) express linear softening models that are described by maximum traction and a critical energy release rate. Also, the bilinear traction-displacement curve (Reedy et al. 1997) has the benefit of simplicity for FEM implementations via an “interface element” or “interface contact” for both crack initiation and growth.

Swaminathan et al. (2006) have explained bilinear traction-displacement relations in both normal and tangential directions for micromechanical composites with fiber-matrix debonding. This model has been in acceptable agreement with experiments for composites illustrated in Li and Ghosh (2004) and Chandra (2002).

The traction (T)—separation (δ) relation in the bilinear model is defined as

$$t = \begin{cases} \frac{t^0}{\delta^0} \delta & \text{if } \delta \leq \delta^0 \\ \frac{t^0}{\delta^0 - \delta^f} (\delta - \delta^f) & \text{if } \delta^0 < \delta \leq \delta^f \\ 0 & \text{if } \delta > \delta^f \end{cases} \quad (7)$$

where t^0 and δ^0 are the maximum cohesive strength and the corresponding strain, δ^f is the maximum strain before the final fracture, see Fig. 3.

Moreover, Mixed-mode damage criteria were implemented in the investigations where the damage behavior depends on both Mode I and Mode II damage as shown in Fig. 3. Benzeggagh–Kenane (BK) fracture criterion (Benzeggagh and Kenane 1996) was employed to define mixed-mode damage for micromechanical RVE, and is given by:

$$G_c = G_{IC} + (G_{IIC} - G_{IC}) \left(\frac{G_{II}}{G_T} \right)^\eta \quad (8)$$

where $G_T = G_I + G_{II}$ and the exponent η is the B–K power law parameter.

Fiber-matrix debonding is included in the simulation by the cohesive zone model in terms of a mix-mode bilinear traction–separation law. In this paper, the elastic stiffness is selected as $K_{nm} = K_{ss} = 10^8 \frac{N}{mm^3}$ (Melro 2013; Canal 2012) and interface damage initiates at $t_n^0 = 50$ MPa, $t_s^0 = 75$ MPa (Dávila et al. 2009; Reedy et al. 1997). The fracture energy G for normal and shear traction–separation curves are considered as $G_{IC} = 0.002 \frac{N}{mm}$, $G_{IIC} = 0.006 \frac{N}{mm}$ (Melro 2013). Also, the B–K power law parameter is assumed as $\eta = 1.45$ (Arteiro 2015). Also, the viscosity parameter is assumed to be 0.0005.

5 Results

In this section, the damage behavior of RVEs with 20%, 40%, and 60% fiber volume fractions have been investigated. Also, the effects of parameters such as mesh size, minimum fiber spacing and different parameters of the cohesive zone are discussed.

5.1 Mesh size effect

In general, choosing the correct size of elements is a challenging step that affects the results in finite element analyses. The mesh size should be refined until

the results approach to the certain amounts. Meanwhile, minimizing the size of elements may lead to computational costs or even the divergence of the solution.

Figure 4 shows the stress-strain diagrams for RVEs with 20% and 40% fiber volume fractions consisting of different mesh sizes. Several analyses with mesh sizes were performed with both square and triangular elements. It should be noted that the smaller mesh size is required for the RVEs with higher fiber volume fraction, based on the fact that the fibers are closer to each other in RVEs with higher fiber volume fractions, which results in the regions with higher stress concentration. In all analyses, there is a high correlation between the results obtained from triangular and square elements. Meanwhile, models with triangular elements exhibit better convergence in the damage portion and analyses continue to a higher strain.

In RVEs with 20% fiber volume fraction, the results of the 1 μ m element have a significant error both in the elastic region and in the damage portion, see Fig. 4a. Where the modulus of elasticity derived 6.903 GPa and the maximum strength of the RVE was 67.75 MPa for both triangular and square elements. However, the results converged with the smaller element sizes and in the mesh sizes 0.7, 0.5 and 0.4 μ m, the modulus of elasticity derived 7.960, 7.955 and 7.955 GPa, respectively, and the maximum strength of 62.74, 63.06, and 63.23 MPa with an error less than 0.01 percent for the elastic modulus and 0.2 percent for the maximum strength value. Therefore, in all the modeling of this paper for RVEs with 20% fiber volume fraction, the mesh size is restricted to .7 μ m, for accuracy and optimum solving time.

Also, the results for the RVEs with 40% fiber volume fraction are shown in Fig. 4b. The elasticity modulus for the mesh size of 0.8, 0.4 and 0.2 μ m are derived as 8.103, 9.963, and 9.957 GPa, respectively. According to the results obtained in Fig. 4b, the mesh size of 0.4 μ m was selected for analyses of RVEs with 40% fiber volume fraction.

5.2 Damage behavior of RVEs with different fiber volume fractions

The damage behavior of the RVEs with 20% fiber volume fraction has been investigated, from elastic deformation to their final fracture. As shown in Fig. 5, in low tensile strains $\varepsilon < 0.01$, the stresses are in an elastic

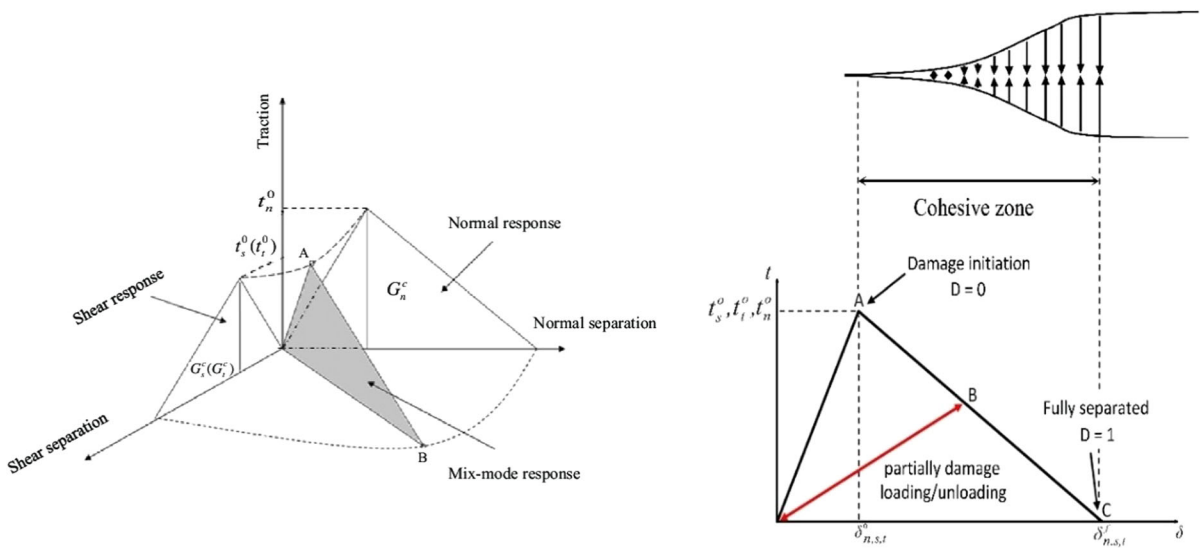


Fig. 3 Bilinear traction-separation laws employed in cohesive element models and mix mode damage evaluation (Zhang 2015)

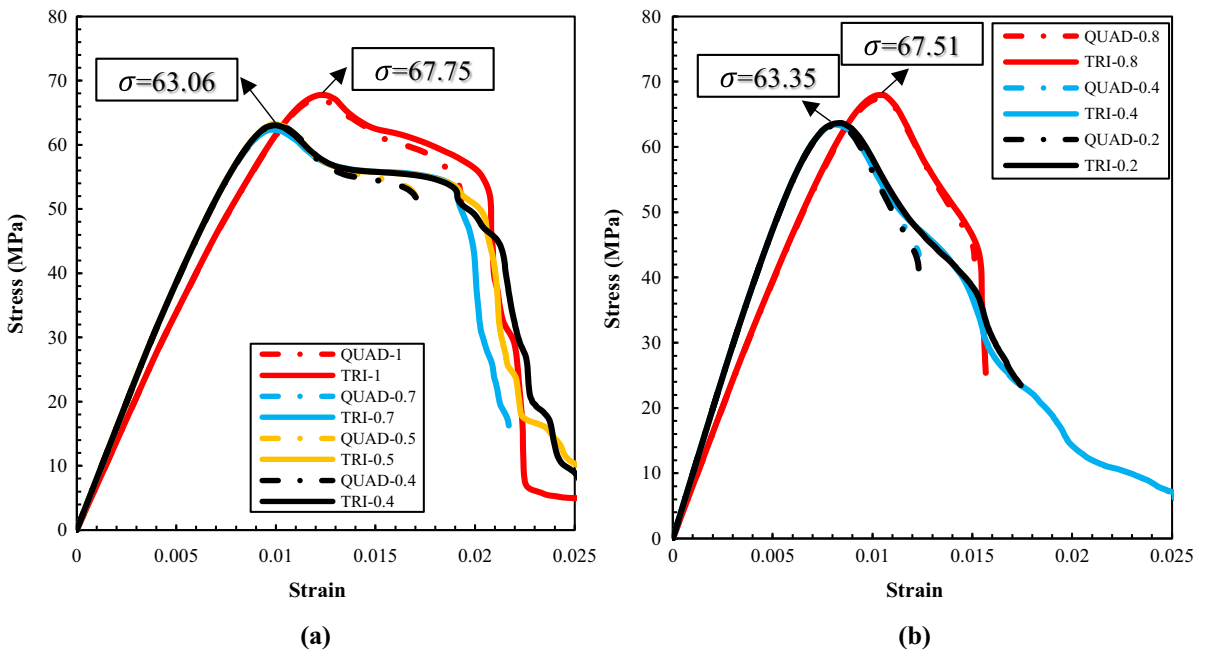


Fig. 4 The effect of mesh size on results for RVEs **a** 20%, **b** 40% fiber volume fraction (the mesh type and its size in μm presented in the legend)

range, so the deformation of the components will be elastic (Fig. 5a). This elastic behavior continues to the climax, $\sigma_{xx} = 62.46$ MPa, in which the force required to separate the fibers from the matrix is sufficient for a cluster of fibers (Fig. 5b). It should be noted that before this stage, due to stress concentration created by ran-

dom fiber arrangement, one or several fibers may experience fiber-matrix debonding, but due to a large number of fibers in the RVE (160 fibers), it does not have an impact on the overall stress-strain curve. In RVEs with 20% fiber volume fraction, the stress field comprises low-stress concentration, so damage domains are

sparse and separated from each other. Thus, the primary damage mode is fiber-matrix debonding in these RVEs (Fig. 5b) and in the following matrix cracks spring up by increasing the strain.

Fiber-matrix debonding is initiated in $\varepsilon_{xx} = 0.01$ and after a drop due to fiber-matrix damage mode the stress-strain diagram will remain almost constant to $\varepsilon_{xx} = 0.018$. In this interval, the cracks opening between the fibers and matrix and the plastic strain in the matrix increase and approach the strain of the crack initiation (point C). In the subsequent step, matrix damage occurs by increasing the strain. These damage modes will develop, and when damage parameters arrive at a value of 1, matrix cracks will emerge (Fig. 5d). At this moment, due to the initiation and growth of matrix cracks, a very small strain change in the RVEs will lead to a significant reduction in their strength.

According to the fiber's arrangement in the RVEs, matrix cracks may be created in several regions simultaneously and expand together. Finally, matrix cracks lead to a dominant crack that crosses the entire RVE dimension (Fig. 5e). As shown in Fig. 5, the final fracture of the RVE occurs at the strain 0.33 (point E).

The behavior of an RVE with 60% fiber volume fraction is investigated in Fig. 6. A greater number of fibers are needed for this fiber volume fraction (478 fiber), so the fibers are expected to pose much closer to each other, which would require a smaller mesh size. As a result, in this section, the computational cost is much higher than the previous analysis. Stress-strain diagram and stress contours for different strain portions are shown in Fig. 6. As shown in Fig. 6a, the stress-strain diagram in this section is different from the behavior of RVEs with 20% fiber volume fraction. In this case, two damage modes of fiber-matrix debonding and matrix cracks will occur simultaneously, indicating the existence of a high-stress concentration in the RVE.

When the RVE with 60% fiber volume fraction is subjected to horizontal strain, in the lower strain (less than 0.007), the elastic behavior for RVE is expected (Fig. 6a) with about 30% reduction in elastic range with respect to RVEs with 20% fiber volume fraction. The elastic region becomes smaller by increasing the fiber volume fraction and the damage modes initiation will occur in smaller strain. The elastic behavior will continue to the strength climax, which is approximately 66 MPa (Fig. 6b). By increasing fiber volume fraction,

the maximum strength does not change markedly compare to the 20% fiber volume fraction (about 3 MPa). This is due to the fact that instead of fiber volume fraction, the maximum strength of the RVE is highly dependent on the properties of the cohesive zone. It is noted that the aim of increasing the fiber volume fraction is mostly about stiffness growth, although the maximum strength is increased slightly. Assuming constant cohesive zone model properties, the RVEs with higher fiber volume fraction approach to this climax in a lower strain due to the higher stiffness. On the other hand, RVEs with higher fiber volume fraction experience fields with higher stress concentrations due to the closer fibers' positions. This may result in matrix crack initiation and final failure in a lower strain.

Fiber-matrix debonding and matrix cracks will occur in RVE by increasing the strain (Fig. 6c). These damages will gradually expand in the RVE and approach each other. The damage growth pattern is highly dependent on the fiber arrangement layouts. In some layouts, a dominant crack is created and developed through the entire RVE dimension and results in final RVE failure. In others, failures occur in different regions and may eventually interconnect or remain apart.

Figure 6d shows that two matrix cracks are formed at the top and bottom of the RVE and expanded toward each other. While in a region close to each other, the presence of a rich fiber region will slow down the growth of the cracks and lead to the failure in a higher strain. Finally, Fig. 6e shows the ultimate fracture of the RVE.

5.3 Random fiber arrangement effects

The fibers arrangement layout has a great effect on the damage behavior of the RVE. For a better understanding of the effect of the randomness of fiber positions on the damage behavior of the RVEs, compression has been done for RVE with random fiber distribution with a non-random composite with constant fiber diameter (equal to the mean of the distribution), and interfiber spacing (also the mean value) for RVE with 40% fiber volume fraction (Fig 7).

Figure 7 demonstrates the effect of fiber randomness on the fracture behavior of RVE. Although in the elastic portion of the loading, the responses of two RVEs are in a reasonable agreement, the damage modes (fiber-matrix debonding and matrix cracks) initiate and

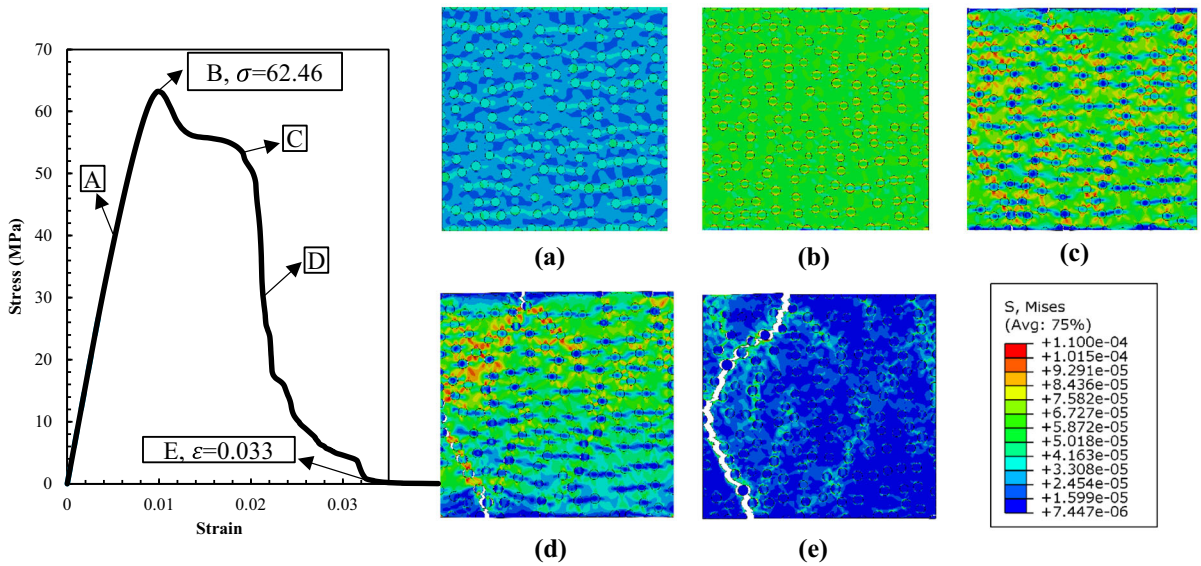


Fig. 5 Stress-strain diagram for an RVE with 20% fiber volume fraction and different Von-Mises contour through final fracture (stress $\times 10^6$ MPa)

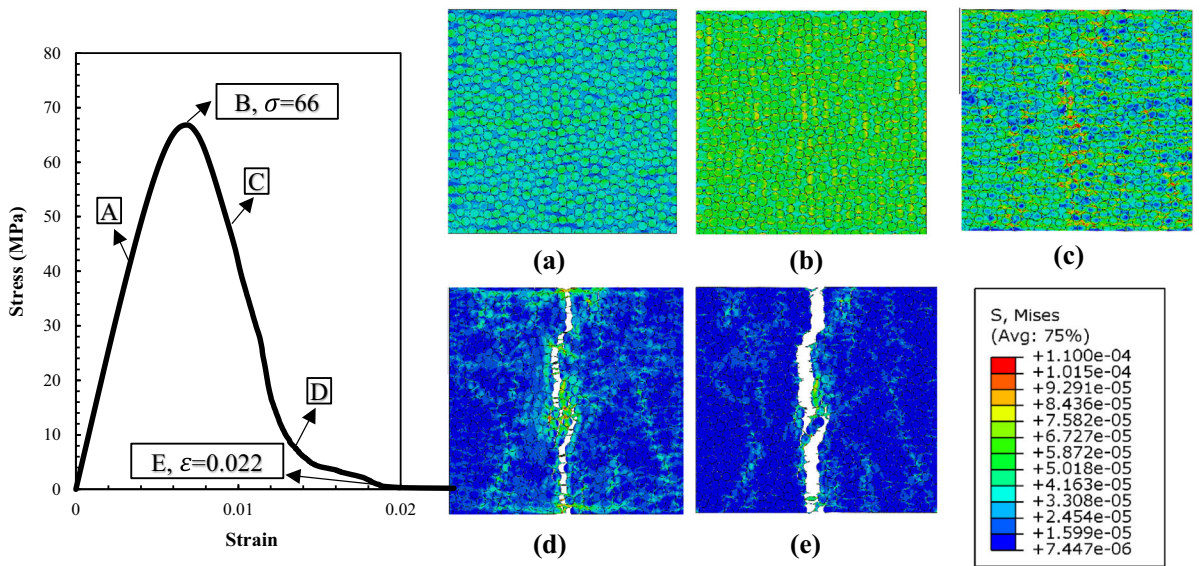


Fig. 6 Stress-strain diagram for an RVE with 60% fiber volume fraction and different Von-Mises contour through final fracture (stress $\times 10^6$ MPa)

propagate in smaller strains for RVE with regular fiber arrangement. In RVE with regular fiber arrangement, the fibers posed beside each other in an orderly pattern, so the areas with high-stress concentration also arrange vertically in the proximity of each other in horizontal transverse tension loading.

Moreover, after the fiber-matrix debonding developed enough to create matrix cracks, small cracks have been initiated for a column of fibers in the same position. As these positions are posed in a vertical position in this sort of loading, the RVE final fracture occurs a single main vertical matrix crack which has been created by reaching those small cracks to each other. The

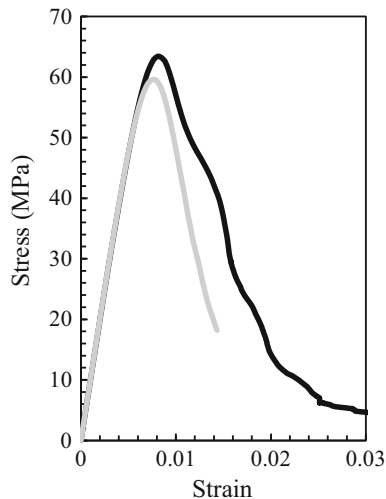


Fig. 7 Stress-strain diagrams for an RVEs with regular (grey graph) and random (black graph) fiber distribution with 40% fiber volume fraction

existence of this main vertical crack in the RVE is the best evidence to demonstrate why the overall stiffness of RVE diminishes a sharper rate, and the final fracture happens in a smaller strain.

As a rule of thumb, RVEs with regular fiber volume fractions experience a lower maximum overall strength and ultimate fracture strain rather than RVEs with random fiber distributions.

Regarding the fact that the random layout of the fibers is generated in the RVEs with reasonable large dimensions (50 times the radius of the fiber), it is noted that the damage behavior of the RVE varies for different fibers configuration layouts (Fig. 8).

To evaluate all the graphs of Fig. 8, it is concluded that the behavior of RVEs defer in different random fiber arrangement schemes and fiber volume fractions. This is due to the fiber spacing and the stress concentration between them. The higher stress concentration leads to a lower fracture strain for the RVE. According to the diagrams presented in Fig. 8 for 20%, 40%, and 60% fiber volume fractions, the convergence of results is very high up to strains of 0.012, 0.01 and 0.009, respectively.

The elastic behavior can be achieved by such an RVE with a dimension that is only several times the fiber radius with acceptable accuracy. Whereas, if the behavior of the matrix is considered to be elastoplastic, this size should increase. In general, the more complex the behavior of the material is, the larger size

of the RVE is needed. However, it seems that even by RVEs with great dimensions, the damage portion of the stress-strain graph still exhibit variation due to the different random fiber distributions. That's because even by using large dimension RVEs, the matrix crack and debondings damage are scattered in different configurations and results various responds. Apparently, boundary conditions are also very effective in achieving accurate results with smaller RVEs. In this study, the periodic boundary conditions have been used for better convergence.

In Fig. 8a, RVEs with 20 fiber volume fractions, it is perceived that the results are highly converged up to the end of the strength loss due to the separation of fibers from the matrix in RVEs with 20% fiber volume fraction and different fiber layouts. However, as the matrix cracks initiate, the results are coming apart from each other but they still follow a unique trend.

The behavior of the RVEs with 40% fiber volume fraction follows a different manner (Fig. 8b).

The integrity of results similar to RVEs with 20% fiber volume fraction is fully attained until the end of the separation of the fibers from the matrix, while in the matrix cracking strain portion, the results are clearly various.

In RVEs with 60% fiber volume fraction, the results variation becomes notable in strain range greater than $\varepsilon_{xx} = 0.009$, Fig. 8c. In these RVEs, as well as the RVEs with 40% fiber volume fraction, due to the random fiber arrangements, the matrix cracks scheme is a significant factor, which affects the variation of the overall behavior of RVEs. The point that should be considered about the RVEs with 60% volume fraction is that the fibers are very closely aligned, which result in high-stress concentration. This high-stress concentration will result in the final fracture of the RVE in a lower strain. Therefore, the difference in the diagrams in these RVEs, just like the RVEs with 40% fiber volume fraction, is related to the arrangement layouts of different fibers.

The variation in the stress-strain diagrams after the fiber-matrix debonding portion is due to the crack's propagation styles. Regarding the different random fiber distributions, the stress contours are disparate for each RVEs. The variation of stress contours results in many matrix crack initiation and propagation schemes, Fig. 9. In some RVEs, a dominant matrix crack was created and crossed the entire length of the RVE, indicating that the strength is lost quickly. While in others,

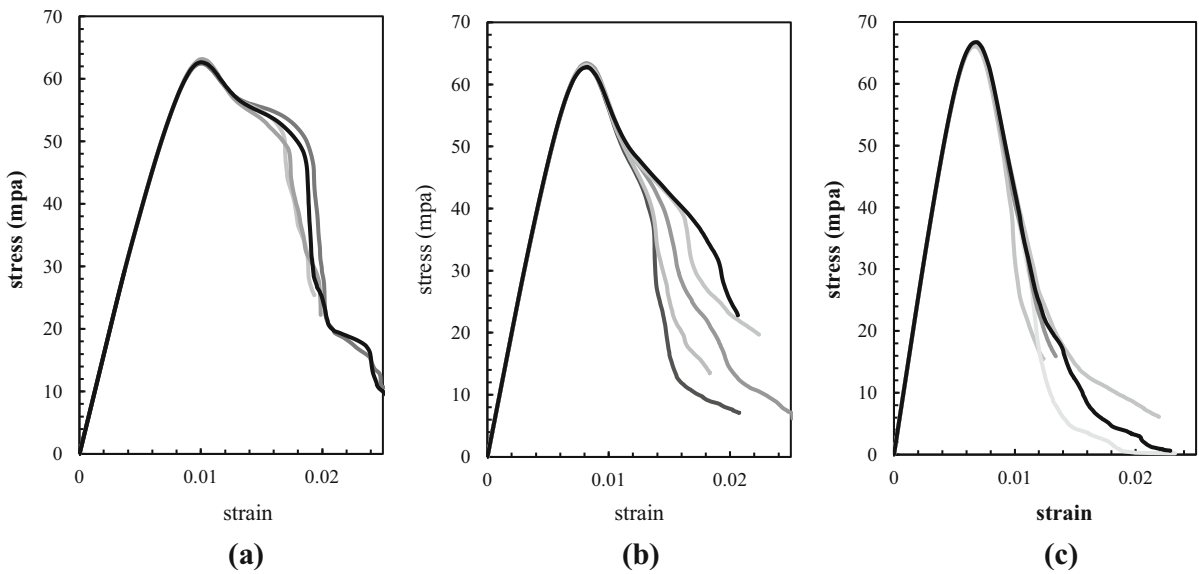


Fig. 8 The effect of different random fiber distribution on damage behavior of the RVEs with **a** 20%, **b** 40%, and **c** 60% fiber volume fractions

several matrix cracks developed and propagated concurrently without reaching to each other, so its strength decreases at a gradual rate. The effect of random fiber distribution on the crack scheme is demonstrated in Fig. 9 for RVEs with 20%, 40%, and 60% fiber volume fractions.

It is observed that even by using large RVEs (the dimension of the RVEs are 50 times of fiber radius), the fiber positions affect both the damage parameter growth during the matrix crack propagation, and the final fracture strain of the RVEs.

5.4 Cohesive zone parameters effects

In this section, the various parameters that affect the behavior of the cohesive zone which forms the separation of the fibers-matrix interface are studied. For two fiber volume fractions, 20% and 40%, the variation of all parameters has been investigated (Fig. 10). For this purpose, two RVEs with 20% and 40% fiber volume fractions are chosen, and for each analysis, only one (the selected) parameter has changed with respect to the original model.

The twenty percent variation of different parameters which is introduced in the cohesive zone such as the final shear strength t_s^0 , the failure energy in the normal and shear direction (G_{IC}, G_{IIC}), and the B-K rule

parameter η do not have a considerable change in the damage behavior of the RVEs for both 20% and 40% fiber volume fractions (Fig. 10a). In Fig. 10a, the black graphs represent the initial state with no change.

Since the RVEs are under horizontal strain, normal strength (t_n^0) is the dominant cohesive zone parameter that has a significant role in the damage behavior of RVEs. The damage behavior of RVEs affecting twenty percent change in the normal strength (t_n^0) of the cohesive zone is presented in Fig. 10b, c. The noteworthy point is that changing the normal strength parameter (t_n^0) has a strong effect only in a particular range of strain, the part related to the interface debonding, and the other portions of the graph almost remain constant.

The maximum cohesive strength in the normal direction (t_n^0) determines the total strength of the RVE. Since the fiber matrix debonding is the first damage mode that occurs in the RVE by increasing the strain and this separation in the fiber matrix interface depends only on the ultimate cohesive strength in the normal direction (t_n^0), the increase of (t_n^0) leads to a linear increase of total strength of the RVE on the range of the tested strengths (Fig. 10b, c). The maximum strength of the RVEs with 20% fiber volume fraction for the normal strength of the cohesive element 40, 45, 50, 55, and 60 MPa are 56.57, 60.23, 63.23, 66.63, and 69.79 MPa, respectively (Fig. 10b). The greater the maximum strength of the RVE,

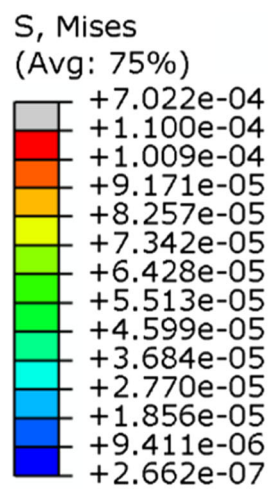
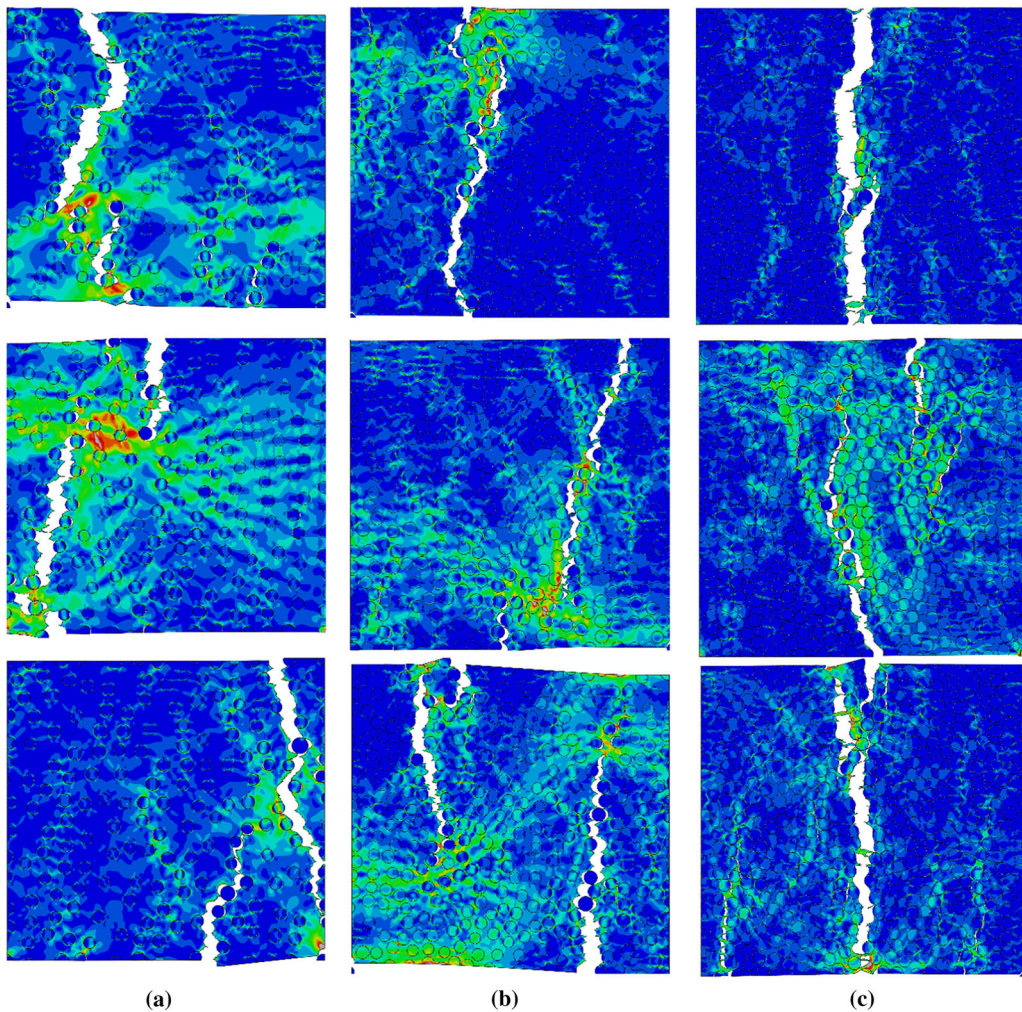


Fig. 9 The effect random fiber distribution on the matrix crack initiation and propagation scheme in RVEs with **a** 20%, **b** 40%, and **c** 60% fiber volume fractions

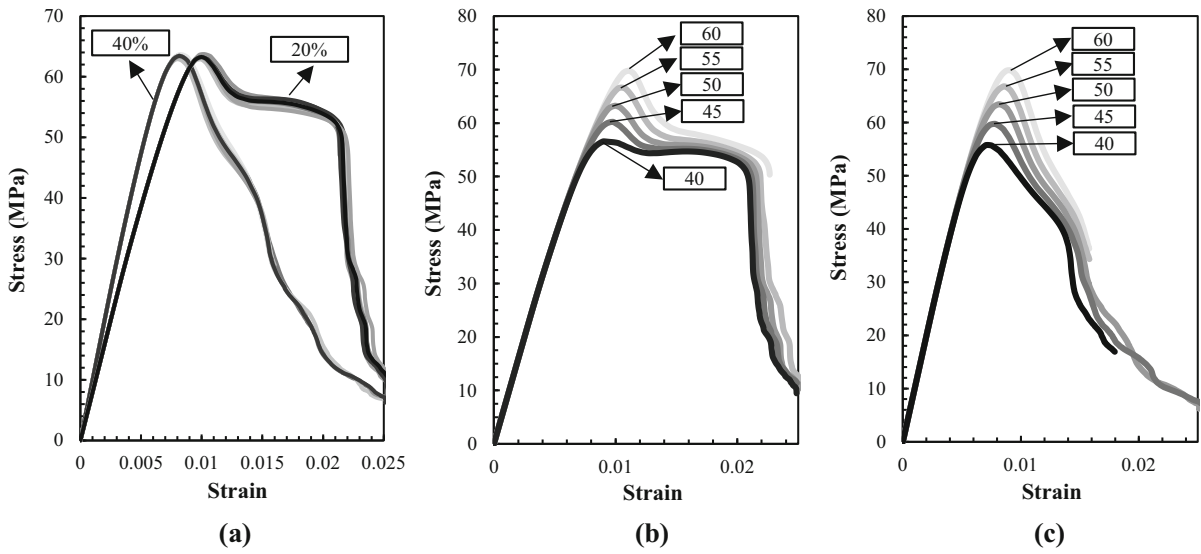


Fig. 10 The effect of cohesive zone parameters on damage behavior of the RVEs **a** The twenty percent variation of t_s^0 , G_{IC} , G_{IIC} , and η **b** Cohesive zone normal strength (t_n^0) varia-

tion for RVEs with 20% volume fraction **c** Cohesive zone normal strength (t_n^0) variation for RVEs with 40% volume fraction

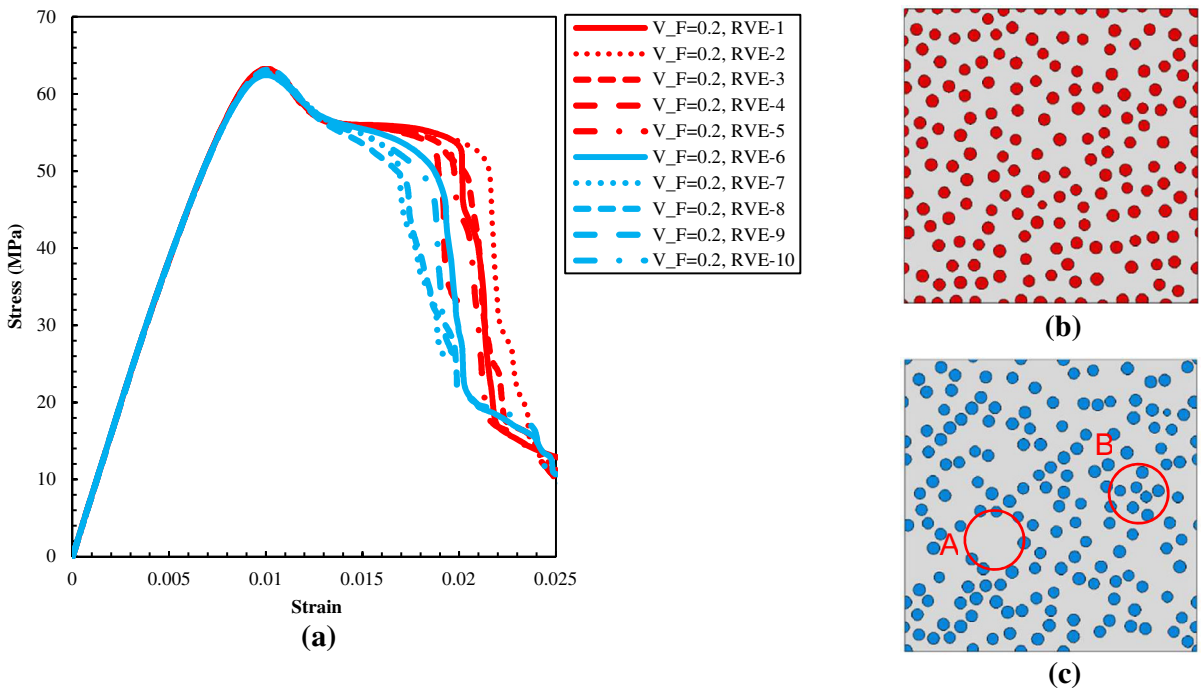


Fig. 11 The effect of fiber neighboring spacing on damage behavior of the RVEs **a** Stress-Strain diagrams, **b** an RVE with a minimum fiber spacing of 3.5 μm , and **c** an RVE with a minimum fiber spacing of 1 μm

the total loss of strength would also be higher after fiber-matrix debonding, consequently, all the RVEs at the matrix cracks initiation point would be at about the same level of strength.

The variation of the maximum strength of the RVEs with 40% fiber volume fraction is similar to that of 20%, so that for the maximum strength of the cohesive element 40, 45, 50, 55, and 60 MPa, the maximum strength of the RVE is 55.76, 59.74, 63.42, 66.78, and 69.82 MPa (Fig. 10c). In this collection, the results are closely related to each other after the total strength loss of RVE, which experience the fiber-matrix separation. This is due to the fact that fiber-matrix debonding are completely formed and the effect of the different cohesive parameters in the modeling has been eliminated.

5.5 Minimum fiber neighboring distance effects

Several parameters influence the behavior of RVEs, such as the minimum neighboring distance between the fibers. This parameter is considered as input data in the code written to generate random fiber distributions. If a larger parameter is chosen, the distribution of the fiber inside RVE would be more uniform, which will result in more uniform stress distribution.

However, the assumed percentage of the fiber volume fraction and the radius of the fiber are two constraints for the range of this distance. Thus, it may impossible to achieve the desired fiber volume fraction by increasing this distance exceedingly. Obviously, the larger the fiber volume fraction is, the smaller the distance that should be considered. On the other hand, the selection of a larger fiber radius can lead to a larger range for determining this distance.

In order to investigate the effect of minimum fiber spacing, ten RVEs with 20% fiber volume fraction are generated with material and geometric properties like the previous sections. The various fiber arrangements in RVEs are assumed random. The first five RVEs, shown in red color in Fig. 11, have a minimum fiber spacing of 3.5 μm which is the largest value that can leads to an RVE with 20% fiber volume fraction. In this series of RVEs, fibers are distributed almost uniform within the matrix. In Fig. 11b, an example of these RVEs is presented with a clear uniform distribution. The second five RVEs are created with the same specifications, but with a minimum fiber spacing of 1 μm . As shown in Fig. 11c, the minimum fiber spacing causes a higher

fiber density in some areas than the other part of the RVE so the uniformity of distribution is eliminated. For example, in circle A shown in Fig. 11c, there are no fibers, while in circle B with the same size, the accumulation of seven fibers is placed.

Since the dimensions of RVEs are considered much greater than fiber radius (fifty times), various fiber distributions, as well as minimum fiber spacing do not affect the behavior of the RVEs in the elastic range, and the results of the RVEs are in high convergence. It should be noted that these parameters completely affect the elastic behavior of the RVEs when the dimensions of the RVE aren't taken adequate large.

In Fig. 11a, the behavior of the RVEs under horizontal strain is introduced. As illustrated previously, RVEs with greater minimum fiber spacing (RVEs of 1 to 5) have more uniform stress fields, and consequently, the matrix cracks appear in a larger strain. In contrast, RVEs with a smaller minimum fiber spacing (RVEs of 6 to 10) experience a matrix crack and final rupture in a smaller strain due to greater stress concentration. In RVEs with a minimum fiber spacing of 1 μm (blue diagrams), matrix cracking occurred exactly after the drop in overall strength due to fiber separation from the matrix at .02 strain. While in RVEs with a minimum fiber spacing of 3.5 μm (red diagrams), matrix cracks occur in the strain of 0.03 with a tolerance of 0.01 strain.

There is not any notable change in the overall strength of the ten RVEs. In other words, as seen in Fig. 11a, the variation of the minimum fiber spacing does not have any significant effect on the overall strength of the RVEs. However, the average of overall strength in the RVEs with a smaller minimum fiber spacing is about 1% less than the other RVEs, which is negligible.

6 Conclusion

A new method for the automatic generation of unidirectional long fiber reinforced composite RVEs with high fiber volume fraction and random fiber distribution is presented in this paper. The method gives the user a relatively high-level of control through several input variables it requires such as fiber volume fraction, fiber and RVE sizes, normal distribution for the fiber's radii, and minimum fiber neighboring spacing. This scheme is suitable for displacement-controlled finite element

analyses; thus, it can be incorporated with commercial finite element codes for composite materials analyses.

The damage behavior of RVEs with various fiber volume fractions has been discussed. As the regions with high-stress concentrations are created in RVEs with higher fiber volume fraction, smaller elements are needed to analyze accurately. It is shown that triangle elements are more appropriate and have a higher convergence. The simulation results indicate that the damage behavior under transverse tension is initiated by fiber-matrix debonding and then followed by matrix damage. However, in RVEs with high fiber volume fraction, the two damage modes initiate and propagate simultaneously. It is shown that the randomness position of the fibers does not affect the maximum strength of the RVE and the corresponding strain. Furthermore, the way matrix cracks propagate in the matrix controls the final RVE's fracture strain. Moreover, in transverse tensile loading, the maximum normal strength is the dominant cohesive parameter for the fiber-matrix debonding. Minimum fiber neighboring distance is another parameter that affects the matrix crack initiation strain. In other words, the minimum fiber neighboring distance is directly related to the strain of matrix crack initiating in the RVE.

References

- Abaqus A (2003) Standard user's manual. ABAQUS Inc
- Arteiro A et al (2015) Micro-mechanical analysis of the effect of ply thickness on the transverse compressive strength of polymer composites. *Compos Part A Appl Sci Manuf* 79:127–137
- Asp Leif E, Berglund LA, Gudmundson P (1995) Effects of a composite-like stress state on the fracture of epoxies. *Compos Sci Technol* 53(1):27–37
- Asp LE, Berglund LA, Talreja R (1996) A criterion for crack initiation in glassy polymers subjected to a composite-like stress state. *Compos Sci Technol* 56(11):1291–1301
- Asp LE, Berglund LA, Talreja R (1996) Prediction of matrix-initiated transverse failure in polymer composites. *Compos Sci Technol* 56(9):1089–1097
- Baby S (2015) Homogenization based continuum damage model for composites. Johns Hopkins University, Diss
- Barbero EJ (2013) Finite element analysis of composite materials using ANSYS. CRC Press, Boca Raton
- Benzeggagh ML, Kenane MJCS (1996) Measurement of mixed-mode delamination fracture toughness of unidirectional glass/epoxy composites with mixed-mode bending apparatus. *Compos Sci Technol* 56(4):439–449
- Böhm HJ (2020) A short introduction to basic aspects of continuum micromechanics. Cdl-fmd Report 3
- Camanho PP, Davila CG, Moura De MF (2003) Numerical simulation of mixed-mode progressive delamination in composite materials. *J Compos Mater* 37(16):1415–1438
- Canal LP et al (2012) Intraply fracture of fiber-reinforced composites: microscopic mechanisms and modeling. *Compos Sci Technol* 72(11):1223–1232
- Chandra N et al (2002) Some issues in the application of cohesive zone models for metal-ceramic interfaces. *Int J Solids Struct* 39(10):2827–2855
- Clyne TW, Hull D (2019) An introduction to composite materials. Cambridge University Press, Cambridge
- Daniel T et al (2006) Determination of the critical size of a statistical representative volume element (SRVE) for carbon reinforced polymers. *Acta Materialia* 54(13):3471–3484
- Dávila CG, Rose CA, Camanho PP (2009) A procedure for superposing linear cohesive laws to represent multiple damage mechanisms in the fracture of composites. *Int J Fract* 158(2):211–223
- Gamstedt EK, Sjögren BA (1999) Micromechanisms in tension-compression fatigue of composite laminates containing transverse plies. *Compos Sci Technol* 59(2):167–178
- González C, Llorca J (2007) Mechanical behavior of unidirectional fiber-reinforced polymers under transverse compression: microscopic mechanisms and modeling. *Compos Sci Technol* 67(13):2795–2806
- Guild F (2004) Toughening mechanisms in rubber modified thermosets. The 27th annual meeting of adhesive society
- Han G et al (2015) Microscopic progressive damage simulation and scale-span analysis of cross-ply laminate based on the elastic-plastic theory. *Appl Compos Mater* 22(1):1–12
- Hollaway LC (2010) A review of the present and future utilization of FRP composites in the civil infrastructure with reference to their important in-service properties. *Construct Build Mater* 24(12):2419–2445
- Ismail Yaser, Yang Dongmin, Ye Jianqiao (2016) Discrete element method for generating random fibre distributions in micromechanical models of fibre reinforced composite laminates. *Compos Part B Eng* 90:485–492
- Li S, Ghosh S (2004) Debonding in composite microstructures with morphological variations. *Int J Comput Methods* 1(01):121–149
- Maligno AR (2008) Finite element investigations on the microstructure of composite materials. Diss. University of Nottingham
- Masaki H et al (2009) Effect of fiber array irregularities on microscopic interfacial normal stress states of transversely loaded UD-CFRP from viewpoint of failure initiation. *Compos Sci Technol* 69(11–12):1726–1734
- Melro AROS (2011) Analytical and numerical modelling of damage and fracture of advanced composites
- Melro AR et al (2013) Micromechanical analysis of polymer composites reinforced by unidirectional fibres: part I-constitutive modelling. *Int J Solids Struct* 50(11–12):1897–1905
- Melro AR, Camanho PP, Pinho ST (2008) Generation of random distribution of fibres in long-fibre reinforced composites. *Compos Sci Technol* 68(9):2092–2102
- Mishnaevsky L Jr, Gaoming D (2014) Hybrid carbon/glass fiber composites: micromechanical analysis of structure-damage resistance relationships. *Comput Mater Sci* 81:630–640

- Nguyen V-D et al (2012) Imposing periodic boundary condition on arbitrary meshes by polynomial interpolation. *Comput Mater Sci* 55:390–406
- Palizvan M, Mohammad HS, Mohammad TA (2020) Effect of interface properties on micromechanical damage behavior of fiber reinforced composites. *Mater Today Commun* 23:100856
- Reedy ED Jr, Mello FJ, Guess TR (1997) Modeling the initiation and growth of delaminations in composite structures. *J Compos Mater* 31(8):812–831
- Romanov V et al (2013) Statistical analysis of real and simulated fibre arrangements in unidirectional composites. *Compos Sci Technol* 87:126–134
- Romanov V, Lomov SV, Swolfs Y, Orlova S, Gorbatikh L, Verpoest I (2013) Statistical analysis of real and simulated fibre arrangements in unidirectional composites. *Compos Sci Technol* 87:126–134
- Soden PD, Hinton MJ, Kaddour AS (1998) Lamina properties, lay-up configurations and loading conditions for a range of fibre-reinforced composite laminates. *Compos Sci Technol* 58(7):1011–1022
- Soni Ganesh et al (2014) Study of localized damage in composite laminates using micro–macro approach. *Compos Struct* 113:1–11
- Soutis C (2005) Fibre reinforced composites in aircraft construction. *Prog Aeronaut Sci* 41(2):143–151
- Swaminathan S, Pagano NJ, Ghosh S (2006) Analysis of interfacial debonding in three-dimensional composite microstructures. *J Eng Mater Technol* 128(1):96–106
- Thomas H et al (2006) Evaluation of interfacial strength in CF/epoxies using FEM and in-situ experiments. *Compos Part A Appl Sci Manuf* 37(12):2248–2256
- Totry E, González C, LLorca J (2008) Failure locus of fiber-reinforced composites under transverse compression and out-of-plane shear. *Compos Sci Technol* 68(3–4):829–839
- Trias D et al (2006) Random models versus periodic models for fibre reinforced composites. *Comput Mater Sci* 38(2):316–324
- Turon A et al (2006) A damage model for the simulation of delamination in advanced composites under variable-mode loading. *Mech Mater* 38(11):1072–1089
- Vaughan TJ, McCarthy CT (2010) A combined experimental-numerical approach for generating statistically equivalent fibre distributions for high strength laminated composite materials. *Compos Sci Technol* 70(2):291–297
- Vaughan TJ, McCarthy CT (2011) Micromechanical modelling of the transverse damage behaviour in fibre reinforced composites. *Compos Sci Technol* 71(3):388–396
- Xia Z, Zhang Y, Ellyin F (2003) A unified periodical boundary conditions for representative volume elements of composites and applications. *Int J Solids Struct* 40(8):1907–1921
- Yang L et al (2012) Microscopic failure mechanisms of fiber-reinforced polymer composites under transverse tension and compression. *Compos Sci Technol* 72(15):1818–1825
- Yang L et al (2013) A new method for generating random fibre distributions for fibre reinforced composites. *Compos Sci Technol* 76:14–20
- Yang L et al (2015) Micromechanical modelling and simulation of unidirectional fibre-reinforced composite under shear loading. *J Reinforced Plast Compos* 34(1):72–83
- Yang L (2016) Effects of triangle-shape fiber on the transverse mechanical properties of unidirectional carbon fiber reinforced plastics. *Compos Struct* 152:617–625
- Zhang C et al (2015) Progressive damage simulation of triaxially braided composite using a 3D meso-scale finite element model. *Compos Struct* 125:104–116
- Zhang X, O'Brien DJ, Ghosh S (2019) Parametrically homogenized continuum damage mechanics (PHCDM) models for composites from micromechanical analysis. *Comput Methods Appl Mech Eng* 346:456–485

Publisher's Note Springer Nature remains neutral with regard to jurisdictional claims in published maps and institutional affiliations.